First-principles study of electron-phonon interactions and transport in anatase TiO$_2$

Youngho Kang [1], Hartwin Peelaers,[1,2] and Chris G. Van de Walle[1,*]

^{1}*Materials Department, University of California, Santa Barbara, California 93106-5050, USA*

^{2}*Department of Physics and Astronomy, University of Kansas, Lawrence, Kansas 66045, USA*

Electron transport in anatase TiO$_2$, which has important applications in oxide electronics and photocatalysis, is still poorly understood. We investigate the electron mobility in anatase TiO$_2$ by performing first-principles calculations of electron and phonon spectra as well as electron-phonon coupling. The formation of *large polarons* (quasiparticles formed by electrons interacting with phonons in a polar medium) leads to a renormalization of the electronic band structure, which we address using many-body perturbation theory. We correlate the lowering of the mobility of these quasiparticles to the renormalization of band velocities due to the electron-phonon interaction. These results explain why the mobility decreases with increasing temperature, as observed in experiments.

DOI: 10.1103/PhysRevB.100.121113

The anatase phase of titanium dioxide (TiO$_2$) has attracted a lot of attention due to its rich physics and important applications. As a transparent conductor it can be used in solar energy harvesting and flat-panel displays [1]; n-type-doped TiO$_2$ is highly transparent and has shown electrical conductivity comparable to that of Sn-doped In$_2$O$_3$ (ITO), which is the most widely used transparent conductor [1,2]. In addition, TiO$_2$ is known to have excellent photocatalytic capabilities [3]. Recent studies show that the electrical transport is important for the overall efficiency of catalysis: The better performance of anatase compared to rutile (another polymorph of TiO$_2$) was attributed to the difference in mobility between the two phases [4].

Despite the evident importance of the electronic conductivity, the dominant carrier transport mechanism in anatase TiO$_2$ is still controversial—in particular, whether it is based on band electrons or on small polarons. The conduction mechanism has previously been investigated using density functional theory (DFT). It was found that due to the strong electron-phonon interaction excess electrons localize at Ti^{3+} sites, forming *small polarons* [5–7]. Based on this result, hopping was suggested as the main conduction mechanism. Small polarons, however, turned out to be energetically unfavorable compared to delocalized states in calculations where orbital-dependent external potentials were added to obey Koopmans' theorem [8]. Furthermore, transport measurements show that the mobility exceeds 10 cm^2/V s at room temperature; in addition, the mobility decreases with increasing temperature for $T > 50$ K [9]. This experimental result contradicts the small-polaron hopping mechanism, which gives rise to much lower mobilities ($\ll 1$ cm^2/V s) and should show an *increase* in mobility with increasing temperature (based on the increased likelihood of overcoming the hopping barriers at higher temperatures).

While small-polaron hopping cannot provide a satisfactory explanation of the experimental results, the strong electron-phonon interaction is clearly of importance for the electrical properties, as was demonstrated by angle-resolved photoemission spectroscopy (ARPES) on single crystals of TiO$_2$ [10]. A substantial renormalization of the conduction-band structure was observed, resulting from the coupling of an electron with a lattice distortion and leading to an increase in the effective mass of the charge carriers. This provides evidence that the charge carriers are no longer bare electrons, but behave as an interacting quasiparticle called a *large polaron*, which is an intermediate state between localized small polarons and free electrons.

Electron transport calculations using first-principles methods are typically based on the DFT band structure and assume that this noninteracting electronic structure is not affected by the electron-phonon interaction. This might be a good approximation for materials where the electron-phonon interaction is weak, but the ARPES experiments indicate that in the case of anatase TiO$_2$ it is necessary to include the impact of the electron-phonon interaction on the band structure.

In the present Rapid Communication, we investigate the electron-phonon interaction and transport in anatase TiO$_2$ using first-principles calculations combined with many-body perturbation theory. This approach allows us to examine the effect of band-structure renormalization on the electron mobility and thus go beyond the typical assumption of a rigid band structure. The renormalization of the band structure leads to slower velocities of large polarons compared to bare electrons. Subsequent mobility calculations using Boltzmann transport theory show a striking impact on transport: The renormalization of velocities leads to a reduction in mobility by up to 54% compared to the "bare" mobility. The resulting mobility also decreases substantially with temperature.

We perform DFT calculations using the QUANTUM ESPRESSO package [11] with the local density approximation (LDA) exchange-correlation functional [12], and ultrasoft pseudopotentials [13] in which the Ti semicore 3s and 3p
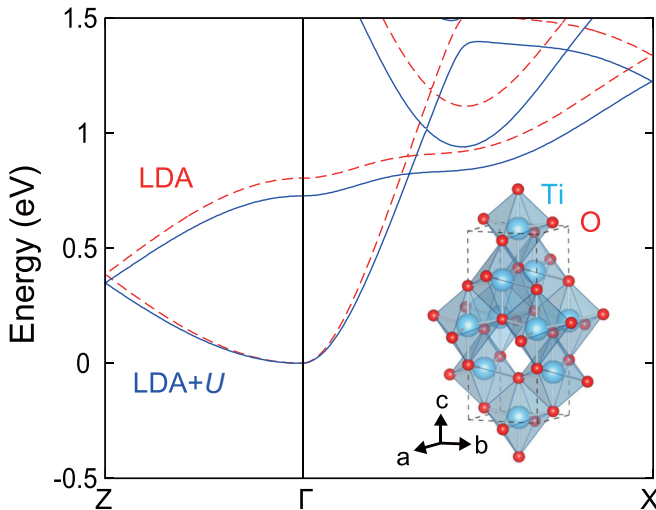
FIG. 1. Conduction-band structure of anatase TiO_2 calculated using LDA (dashed red line) and LDA $+ U$ (solid blue line), based on the optimized geometry obtained with LDA, and plotted along high-symmetry lines of the BZ for the primitive cell. The conduction-band minimum is used as the energy reference in both cases. The inset shows the conventional cell of anatase TiO_2; large blue spheres are Ti atoms, small red spheres O atoms.

states are treated as valence electrons. The plane-wave basis has a cutoff of 50 Ry and we use a $6 \times 6 \times 6$ special k-point grid. The phonon spectrum is calculated using density functional perturbation theory (DFPT) [14] on a $4 \times 4 \times 4$ q-point grid, and interpolated along symmetry lines of the Brillouin zone (BZ).

DFT-LDA provides good structural properties, including phonon dispersion curves (as we will show below), but for the electronic structure a better description of Ti-d-derived conduction-band states is needed. We therefore perform LDA $+ U$ calculations, with the on-site Coulomb energy $U = 3.3$ eV obtained self-consistently using a linear-response approach [15].

Anatase TiO_2 is a band insulator with a tetragonal crystal structure and the $I4_1/amd$ space group as shown in the inset of Fig. 1. The calculated lattice parameter of the primitive cell is 5.42 Å, in good agreement with the experimental value of 5.45 Å [16]. Each Ti atom is surrounded by a slightly distorted oxygen octahedron. The crystal field of these distorted octahedra lifts the degeneracy of the t_{2g} states. As a consequence, the lowest conduction band is derived mainly from d_{xy} states, leading to a highly anisotropic band structure: Dispersion is much stronger along Γ-X than along Γ-Z (Fig. 1). The next-higher conduction-band states have mainly d_{yz} and d_{zx} character. Figure 1 also shows that the conduction bands obtained with LDA $+ U$ show less dispersion than those obtained with LDA. The quality of the LDA $+ U$ band structure is confirmed by the agreement of the electron effective mass obtained with LDA $+ U$ ($0.44m_e$ for the in-plane direction) with a value calculated using a hybrid functional ($0.42m_e$) [17]. The LDA value is $0.37m_e$.

Anatase TiO_2 has 6 atoms in the primitive cell, leading to 18 phonon modes (3 acoustic $+$ 15 optical modes).
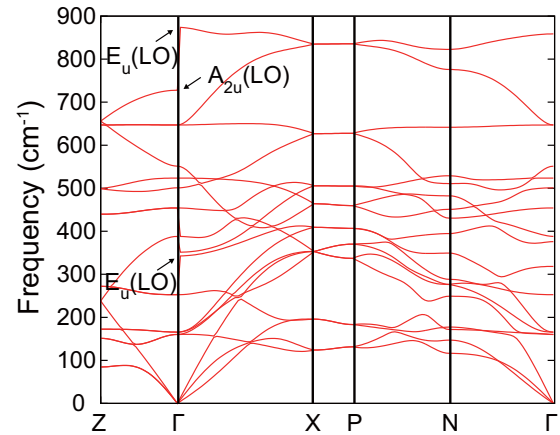

FIG. 2. Calculated phonon band structure of anatase TiO_2 using the LDA functional.

Among them, three pairs of polar optical modes consisting of transverse (TO) and longitudinal (LO) modes can be identified by group theory. Lattice vibrations corresponding to polar LO modes generate a macroscopic electric field at long wavelengths. This causes the splitting of the polar LO and TO modes at the zone center as shown in Fig. 2; in E_u modes ions oscillate in the (a-b) plane, while in the A_{2u} mode they oscillate along the c axis. LO-TO splitting for E_u modes therefore occurs only for phonon wave vectors $\mathbf{q}$ with nonzero x or y components (e.g., along the Γ-X direction), and for A_{2u} modes the LO-TO splitting only occurs for $\mathbf{q}$ with a nonzero z component (e.g., along the Γ-Z line). The calculated frequencies of the optical modes at Γ are in good agreement with experiment, as shown in Table I [18,19].

The coupling of an electron to lattice vibrations can lead to different types of polaron states in solids. An electron placed in a continuous polarizable medium can form a large polaron via coupling to polar LO modes. In contrast to a small polaron, in which an electron is localized on a few atomic sites accompanied by a significant lattice distortion, a large polaron is spread over many lattice sites with a much

TABLE I. Zone-center optical phonon frequencies (in cm^{-1}) for anatase TiO_2 calculated using DFT-LDA and compared with experiment.

Modes	LDA	Expt. [18]	Expt. [19]
E_g	160		144
E_g	166		197
E_u(TO)	253	262	
E_u(LO)	343	366	
A_{2u}(TO)	351	367	
B_{1g}	388		399
E_u(TO)	454	435	
B_{1g}	501		519
A_{1g}	524		513
B_{2u}	551		
E_g	647		639
A_{2u}(LO)	728	755	
E_u(LO)	874	876	

smaller lattice distortion. The atomic displacement due to polar LO modes follows the polaronic motion, effectively dressing the electron. Hence, large polarons move through the lattice similar to free electrons but with a heavier effective mass.

Fröhlich examined the effective mass of a large polaron for an isotropic system with a parabolic band structure and a single LO phonon mode [20]. He derived the dependence of the polaron mass on the electron-phonon coupling strength using perturbation theory. In TiO_2, however, the physical properties are anisotropic and there are multiple LO phonon modes and therefore the Fröhlich approach is inadequate [21]. Here, we use the following Fröhlich-like Hamiltonian as a starting point,

$$H = \sum_{\mathbf{k}} \epsilon_{\mathbf{k}} \hat{c}_{\mathbf{k}}^{\dagger} \hat{c}_{\mathbf{k}} + \sum_{\mathbf{q}} \sum_{\nu} \hbar \omega_{\mathbf{q}\nu} (\hat{a}_{\mathbf{q}\nu}^{\dagger} \hat{a}_{\mathbf{q}\nu} + 1/2)$$
$$+ \frac{1}{\sqrt{V_{\text{cell}}}} \sum_{\mathbf{k}} \sum_{\mathbf{q}} \sum_{\nu} g_{\nu}(\mathbf{q}) \hat{c}_{\mathbf{k}+\mathbf{q}}^{\dagger} \hat{c}_{\mathbf{k}} (\hat{a}_{-\mathbf{q}\nu}^{\dagger} + \hat{a}_{\mathbf{q}\nu}), \quad (1)$$

where $\epsilon_{\mathbf{k}}$ is the energy of an electron in the conduction band with momentum $\mathbf{k}$, $\hat{c}_{\mathbf{k}}^{\dagger}$ and $\hat{c}_{\mathbf{k}}$ are the electron creation and annihilation operators, $\omega_{\mathbf{q}\nu}$ is the LO phonon frequency for the νth polar LO phonon mode with momentum $\mathbf{q}$, $\hat{a}_{\mathbf{q}\nu}^{\dagger}$ and $\hat{a}_{\mathbf{q}\nu}$ are the phonon creation and annihilation operators, and V_{cell} is the volume of the unit cell. We do not assume a single parabolic conduction band but explicitly consider the full band structure obtained from first-principles calculations. The matrix element $g_{\nu}(\mathbf{q})$ measures the strength of electron-phonon coupling and has units of energy. Note that this Hamiltonian only describes polar LO modes, but these modes have the largest electron-phonon coupling compared to the other modes in TiO_2 [22,23].

In the Vogl model [21,24] the electron-phonon matrix element for coupling to long-wavelength LO phonons is

$$g_{\nu}(\mathbf{q}) = i \frac{e^2}{V_{\text{cell}} \varepsilon_0} \sum_{j} \sqrt{\frac{\hbar}{2 M_j \omega_{\mathbf{q}\nu}}} \frac{\mathbf{q} \cdot \overline{\overline{Z}}_j \cdot \mathbf{e}_{j\nu}(\mathbf{q})}{\mathbf{q} \cdot \overline{\overline{\varepsilon}}_{\infty} \cdot \mathbf{q}}, \quad (2)$$

where e is the electron charge, ε_0 the vacuum permittivity, and M_j the atomic mass of atom j. $\overline{\overline{Z}}_j$ is the Born effective charge tensor and $\mathbf{e}_{j\nu}$ the normalized atomic displacement of the jth atom. The electric field created by the polar LO phonons with momentum $\mathbf{q}$ is proportional to $\mathbf{q} \cdot \overline{\overline{Z}}_j \cdot \mathbf{e}_{j\nu}(\mathbf{q})$. The electron-phonon matrix element in Eq. (2) has a $1/|\mathbf{q}|$ dependence due to its long-range nature. As a result, its magnitude around Γ is very large, and therefore the scattering due to polar LO modes dominates the electron transport properties of polar materials compared to those of other types of electron-phonon interactions [25]. It is inversely proportional to $\overline{\overline{\varepsilon}}_{\infty}$, the high-frequency dielectric tensor, which screens the Coulomb interaction. Equation (2) assumes that the Bloch wave functions change smoothly as a function of the electronic wave vector, so that there is no k dependence.

We include the renormalization of electronic band structure due to the electron-phonon interaction via many-body perturbation theory [26]. The electron-phonon self-energy $\Sigma_{\mathbf{k}}(\omega, T)$

is computed within the Fan approximation [27],

$$\Sigma_{\mathbf{k}}(\omega, T) = \sum_{\nu} \int \frac{d\mathbf{q}}{\Omega_{\text{BZ}}} |g_{\nu}(\mathbf{q})|^2 \left[\frac{n_{\mathbf{q}\nu} + 1 - f_{\mathbf{k}+\mathbf{q}}}{\hbar\omega - \epsilon_{\mathbf{k}+\mathbf{q}} - \hbar\omega_{\mathbf{q}\nu} - i\eta} \right.$$
$$\left. + \frac{n_{\mathbf{q}\nu} + f_{\mathbf{k}+\mathbf{q}}}{\hbar\omega - \epsilon_{\mathbf{k}+\mathbf{q}} + \hbar\omega_{\mathbf{q}\nu} - i\eta} \right], \quad (3)$$

where T is the temperature, Ω_{BZ} the volume of the BZ, $n_{\mathbf{q}\nu}$ the Bose-Einstein distribution, and $f_{\mathbf{k}}$ the Fermi-Dirac function. The complex shift in the denominator is added to prevent Eq. (3) from diverging, with η taken to be 0.2 eV. As noted above, the initial electronic band structure is taken from an LDA + U calculation. The BZ integration is performed on a very fine grid of $60 \times 60 \times 60$ q points. For purposes of comparing with experimental transport measurements the electron and phonon occupation factors are obtained for $T = 300$ K and an electron concentration of 10^{18} cm^{-3}.

Assuming the electronic wave functions are not significantly changed due to the electron-phonon coupling, i.e., the off-diagonal elements of the self-energy are negligible, the renormalized band structure can be calculated as

$$\epsilon_{\mathbf{k}}^{p} = \epsilon_{\mathbf{k}} + \text{Re}\, \Sigma_{\mathbf{k}}(\epsilon_{\mathbf{k}}^{p}), \quad (4)$$

where $\epsilon_{\mathbf{k}}^{p}$ is the energy of a polaron state and $\text{Re}\,\Sigma_{\mathbf{k}}$ the real part of the self-energy. Equation (4) has to be solved self-consistently. Combining Eqs. (3) and (4) is equivalent to second-order Brillouin-Wigner perturbation theory for electron-phonon coupling [28]. Here, we introduce a simple and effective approach to solve such an equation. If we assume that the polaron energies are close to the bare electronic energies, the self-energy can be expanded to first order around the bare energy and the solution of Eq. (4) can be approximated as

$$\epsilon_{\mathbf{k}}^{p} = \epsilon_{\mathbf{k}} + Z_{\mathbf{k}} \text{Re}\, \Sigma_{\mathbf{k}}(\epsilon_{\mathbf{k}}), \quad (5)$$

where $Z_{\mathbf{k}}$ is the renormalization factor defined by

$$Z_{\mathbf{k}} = \left[1 - \left(\frac{\partial \, \text{Re}\, \Sigma_{\mathbf{k}}(\omega)}{\hbar \partial \omega} \right)_{\hbar\omega = \epsilon_{\mathbf{k}}} \right]^{-1}. \quad (6)$$

The procedure is illustrated in Fig. 3 for $k = 0$.

As Fröhlich demonstrated, the strong electron-phonon interaction in polar materials increases the mass of the charge carriers, so that polarons will have lower velocities than bare electrons. To evaluate this effect, we calculate the group velocity of polarons $[\mathbf{v}_{\mathbf{k}}^{p} = 1/\hbar(\partial \epsilon_{\mathbf{k}}^{p}/\partial \mathbf{k})]$ and of bare electrons $[\mathbf{v}_{\mathbf{k}} = 1/\hbar(\partial \epsilon_{\mathbf{k}}/\partial \mathbf{k})]$ and plot the ratio $|\mathbf{v}_{\mathbf{k}}^{p}/\mathbf{v}_{\mathbf{k}}|$ in Fig. 4 for states near the conduction-band edge. The results clearly show that the velocities of polaron states are decreased, with values ranging between 75% and 80% of the velocities of bare electrons. The velocity renormalization depends on the energy of the electronic states. However, there is also a strong dependence on the direction of momentum in k space due to the anisotropy of the anatase structure, which explains the multiple data points shown for the same energy in Fig. 4.

The reduction in carrier velocity impacts the mobility. The electrical conductivity tensor $\sigma_{\alpha\beta}$, where α and β denote Cartesian indices, can be calculated using the Boltzmann transport equation within the relaxation time approximation
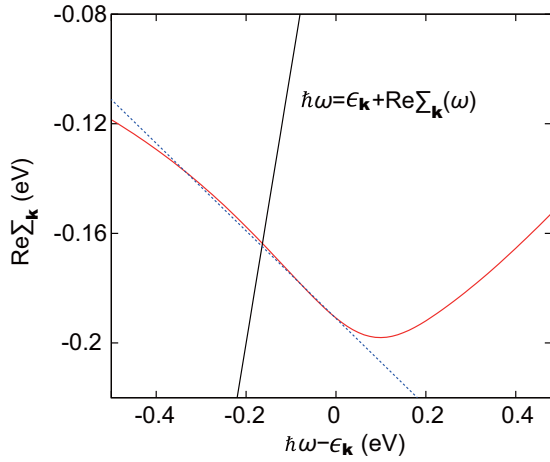
FIG. 3. Real part of the frequency-dependent self-energy for the bottom of the conduction band ($k = 0$). The $x = y$ line gives the amount of the eigenvalue renormalization at the intersection with Re $\Sigma_{\mathbf{k}}$, and the blue dotted line is the linearized self-energy at $\hbar\omega = \epsilon_{\mathbf{k}}$, which approximates the renormalized eigenvalue near the intersection with the $x = y$ line.

as [29]

$$\sigma_{\alpha\beta} = \frac{2e^2}{V_{\text{cell}}} \sum_{\mathbf{k}} w_{\mathbf{k}} \tau_{\mathbf{k}} \left(-\frac{\partial f_{\mathbf{k}}}{\partial E_{\mathbf{k}}} \right) \mathbf{V}_{\mathbf{k},\alpha} \mathbf{V}_{\mathbf{k},\beta}, \quad (7)$$

where $w_{\mathbf{k}}$ is the k-point weight, $E_{\mathbf{k}}$ the energy of the electron carriers, and $\mathbf{V}_{\mathbf{k}}$ the band velocity. We use $E_{\mathbf{k}}$ and $\mathbf{V}_{\mathbf{k}}$ as placeholders for either the bare or renormalized (polaron) energies or velocities. $\tau_{\mathbf{k}}$ is the carrier lifetime arising due to electron-phonon interactions, which in polar materials is dominated by the coupling with LO-phonon modes and can be calculated as follows,

$$\tau_{\mathbf{k}}^{-1} = \frac{2\pi}{\hbar} \sum_{\nu} \sum_{\mathbf{q}} w_{\mathbf{q}} |g_{\nu}(\mathbf{k}, \mathbf{q})|^2$$
$$\times \{ (n_{\mathbf{q}\nu} + f_{\mathbf{k}+\mathbf{q}}) \delta(E_{\mathbf{k}+\mathbf{q}} - E_{\mathbf{k}} - \hbar\omega_{\mathbf{q}\nu})$$
$$+ (1 + n_{\mathbf{q}\nu} - f_{\mathbf{k}+\mathbf{q}}) \delta(E_{\mathbf{k}+\mathbf{q}} - E_{\mathbf{k}} + \hbar\omega_{\mathbf{q}\nu}) \}. \quad (8)$$
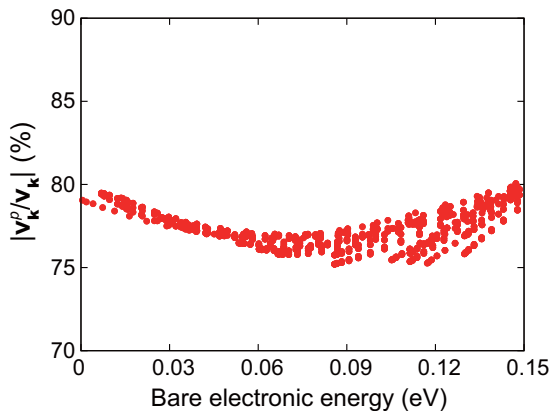

FIG. 4. Energy-dependent velocity renormalization for states near the conduction-band edge.

TABLE II. Calculated mobilities at room temperature for $n = 10^{18}$ cm^{-3}. The conduction band is described either at the LDA or the LDA $+ U$ level, or taking renormalization due to the electron-phonon interaction into account (with the LDA $+ U$ results as the starting point).

LDA		LDA $+ U$		Renormalized	
$\mu_\perp$	$\mu_\parallel$	$\mu_\perp$	$\mu_\parallel$	$\mu_\perp$	$\mu_\parallel$
75	7	56	6	26	2

This expression for the lifetime can be derived from the imaginary part of the self-energy of the polarons [28]. Equation (8) can also be derived from Fermi's golden rule. Note that we do not simply assume the carrier lifetime to be constant, which is a frequently used approximation. Equation (8) explicitly includes the $\mathbf{k}$-point dependence of $\tau_{\mathbf{k}}$, which is important to accurately describe mobilities [25,30]. The mobility tensor $\mu_{\alpha\beta}$ is obtained from $\mu_{\alpha\beta} = \sigma_{\alpha\beta}/ne$, where n is the carrier density. We employ a $60 \times 60 \times 60$ k- and q-point grid to calculate Eqs. (7) and (8). Further increasing the grid size to $100 \times 100 \times 100$ leads to changes in the mobility smaller than 5%. The grid size used here to obtain converged results is smaller than what was found necessary for GaAs and Si [31–34]. This difference in grid size can be attributed to the dispersion of the band structure of the materials investigated; more dispersive bands need finer meshes. For SrTiO$_3$, which has masses comparable to TiO$_2$, Ref. [35] used a denser grid but did not report convergence tests, while Ref. [36] used a grid comparable to our current grid. The delta function in Eq. (8) is replaced by a Gaussian with a width of 0.05 eV. In Eq. (8) we do not include the factor $(1 - \hat{\mathbf{V}}_{\mathbf{k}} \cdot \hat{\mathbf{V}}_{\mathbf{k}+\mathbf{q}})$ that is associated with the effect of directionality in the scattering. Our tests showed that its inclusion changes the mobility by only ~1%. Such a minor impact of the velocity factor on the mobility was previously reported for SrTiO$_3$ [36].

Our calculated values for mobilities at room temperature are listed in Table II. From the analysis of mode-resolved scattering rate, the highest optical mode turns out to dominate the scattering rate. We find that the mobility is ~10 times larger in the direction perpendicular to the c axis ($\mu_\perp$) than in the parallel direction ($\mu_\parallel$). This strong anisotropy arises from the large differences in dispersion of the conduction band in different directions (see Fig. 1). Table II also shows that the calculated mobility depends strongly on the approach used for computing $E_{\mathbf{k}}$. We list values obtained with LDA, LDA $+ U$, and including renormalization due to electron-phonon interactions.

Our results show that the accuracy of conduction-band states affects the mobilities. A proper description of d states, as accomplished in LDA $+ U$, reduces the mobility by as much as 25% compared to the LDA values. If in addition band-structure renormalization is taken into account, the mobility is further reduced by 54%. This reduction is mainly due to the velocity renormalization; indeed, the scattering rates for band-edge states are increased by only ~20% as a consequence of the band renormalization. We note that the conductivity in Eq. (7) depends on the square of the

group velocity. Thus, the velocity renormalization modifies the mobility more significantly than the scattering rate.

The mobility, including the band renormalization effect, decreases with increasing temperature, from $70 \, \mathrm{cm^2/V \, s}$ at 200 K to $26 \, \mathrm{cm^2/V \, s}$ at 300 K for the in-plane direction, consistent with experimental observations [1,9]. We can attribute the decrease to the enhanced LO-phonon scattering at higher temperatures.

Experimentally measured room-temperature values of $\mu_\perp$ range from 17 to $30 \, \mathrm{cm^2/V \, s}$ for $n = 10^{18}$–$10^{20} \, \mathrm{cm^{-3}}$ [1,9]. These values could in principle contain contributions from scattering mechanisms other than LO-phonon scattering. Since the transport measurements were performed on single crystals [9] or epitaxial films [1], we expect the impact of extended defects such as dislocations or grain boundaries to be small. Regarding ionized impurity scattering, we can estimate its contribution based on the experimental data. In Ref. [1] the mobility of an epitaxial sample with $n \sim 10^{20} \, \mathrm{cm^{-3}}$ was measured to be about $100 \, \mathrm{cm^2/V \, s}$ at $T < 100$ K. In a doped semiconductor the mobility at low temperatures is typically dominated by ionized impurity scattering [37]. Thus it is reasonable to assume that the low-temperature mobility of $100 \, \mathrm{cm^2/V \, s}$ mainly arises from ionized impurity scattering. In addition, it is known that the impact of this scattering mechanism decreases as the temperature increases [37]. Accordingly, the mobility limited by only the ionized impurity scattering at room temperature is likely to be higher than $100 \, \mathrm{cm^2/V \, s}$. We can therefore conclude that, even at these high dopant concentrations, ionized impurity scattering does not contribute significantly to the mobility at room temperature, and that LO-phonon scattering will be the main mechanism limiting the mobility. Our results in Table II indicate that it is essential to take renormalization of the band structure into account to accurately describe LO-phonon scattering at room temperature, and this indeed produces values within the experimentally observed range.

Other titanates, such as $SrTiO_3$ and rutile TiO_2, also exhibit mobilities that decrease with increasing temperature [38,39]. Given that these materials also have strong electron-LO-phonon interactions, we expect that large polarons and the resulting band-structure renormalization also play an important role in the transport properties of these materials. The effect may be even larger than in anatase, given that the experimental mobility at room temperature is less than $10 \, \mathrm{cm^2/V \, s}$. A recent study investigated the transport properties of $SrTiO_3$ using the Kubo formula in which the spectral functions of electrons interacting with phonons are considered [40]. The results also show that the change in the band structure due to the strong electron-phonon coupling reduces the mobility (by a factor of 8) compared to that of the bare electron.

In conclusion, we have investigated the mobility of large polarons in anatase TiO_2 using first-principles calculations and the Boltzmann transport equation. We explicitly included the band renormalization due to the electron-phonon coupling within many-body perturbation theory. While the scattering time is modified by 20%, the main effect on mobility stems from velocity renormalization. The large polaron has a 54% lower mobility than the mobility of bare electrons. Our results show that the formation of large polarons plays a crucial role in the electron mobility of anatase TiO_2.

[1] Y. Furubayashi, T. Hitosugi, Y. Yamamoto, K. Inaba, G. Kinoda, Y. Hirose, T. Shimada, and T. Hasegawa, Appl. Phys. Lett. **86**, 252101 (2005).

[2] N. Yamada, T. Shibata, K. Taira, Y. Hirose, S. Nakao, N. L. H. Hoang, T. Hitosugi, T. Shimada, T. Sasaki, and T. Hasegawa, Appl. Phys. Express **4**, 045801 (2011).

[3] A. Fujishima, Nature (London) **238**, 37 (1972).

[4] T. Luttrell, S. Halpegamage, J. Tao, A. Kramer, E. Sutter, and M. Batzill, Sci. Rep. **4**, 4043 (2014).

[5] N. A. Deskins and M. Dupuis, Phys. Rev. B **75**, 195212 (2007).

[6] C. Spreafico and J. VandeVondele, Phys. Chem. Chem. Phys. **16**, 26144 (2014).

[7] D. Kim, B. C. Yeo, D. Shin, H. Choi, S. Kim, N. Park, and S. S. Han, Phys. Rev. B **95**, 045209 (2017).

[8] S. Lany, J. Phys.: Condens. Matter **27**, 283203 (2015).

[9] L. Forro, O. Chauvet, D. Emin, L. Zuppiroli, H. Berger, and F. Levy, J. Appl. Phys. **75**, 633 (1994).

[10] S. Moser, L. Moreschini, J. Jaćimović, O. S. Barišić, H. Berger, A. Magrez, Y. J. Chang, K. S. Kim, A. Bostwick, E. Rotenberg *et al.*, Phys. Rev. Lett. **110**, 196403 (2013).

[11] P. Giannozzi, S. Baroni, N. Bonini, M. Calandra, R. Car, C. Cavazzoni, D. Ceresoli, G. L. Chiarotti, M. Cococcioni, I. Dabo *et al.*, J. Phys.: Condens. Matter **21**, 395502 (2009).

[12] J. P. Perdew and A. Zunger, Phys. Rev. B **23**, 5048 (1981).

[13] D. Vanderbilt, Phys. Rev. B **41**, 7892 (1990).

[14] S. Baroni, S. De Gironcoli, A. Dal Corso, and P. Giannozzi, Rev. Mod. Phys. **73**, 515 (2001).

[15] G. Mattioli, F. Filippone, P. Alippi, and A. Amore Bonapasta, Phys. Rev. B **78**, 241201(R) (2008).

[16] M. Horn, C. Schwebdtfeger, and E. Meagher, Z. Kristallogr. **136**, 273 (1972).

[17] H. A. Huy, B. Aradi, T. Frauenheim, and P. Deák, Phys. Rev. B **83**, 155201 (2011).

[18] R. J. Gonzalez, R. Zallen, and H. Berger, Phys. Rev. B **55**, 7014 (1997).

[19] T. Ohsaka, F. Izumi, and Y. Fujiki, J. Raman Spectrosc. **7**, 321 (1978).

[20] H. Fröhlich, Adv. Phys. **3**, 325 (1954).

[21] C. Verdi and F. Giustino, Phys. Rev. Lett. **115**, 176401 (2015).

[22] V. P. Zhukov and E. V. Chulkov, Phys. Solid State **56**, 1302 (2014).

[23] C. Verdi, F. Caruso, and F. Giustino, Nat. Commun. **8**, 15769 (2017).

[24] P. Vogl, Phys. Rev. B **13**, 694 (1976).

[25] Y. Kang, K. Krishnaswamy, H. Peelaers, and C. G. Van de Walle, J. Phys.: Condens. Matter **29**, 234001 (2017).

[26] G. D. Mahan, *Many-Particle Physics* (Kluwer Academic/ Plenum, New York, 2000).

[27] H. Fan, Phys. Rev. **82**, 900 (1951).

[28] F. Giustino, Rev. Mod. Phys. **89**, 015003 (2017).

[29] J. M. Ziman, *Electrons and Phonons: The Theory of Transport Phenomena in Solids* (Oxford University Press, Oxford, UK, 1960).

[30] K. Krishnaswamy, B. Himmetoglu, Y. Kang, A. Janotti, and C. G. Van de Walle, Phys. Rev. B **95**, 205202 (2017).

[31] T.-H. Liu, J. Zhou, B. Liao, D. J. Singh, and G. Chen, Phys. Rev. B **95**, 075206 (2017).

[32] S. Poncé, E. R. Margine, and F. Giustino, Phys. Rev. B **97**, 121201(R) (2018).

[33] J. Ma, A. S. Nissimagoudar, and W. Li, Phys. Rev. B **97**, 045201 (2018).

[34] J.-J. Zhou and M. Bernardi, Phys. Rev. B **94**, 201201(R) (2016).

[35] J.-J. Zhou, O. Hellman, and M. Bernardi, Phys. Rev. Lett. **121**, 226603 (2018).

[36] B. Himmetoglu, A. Janotti, H. Peelaers, A. Alkauskas, and C. G. Van de Walle, Phys. Rev. B **90**, 241204(R) (2014).

[37] D. Rode, *Semiconductors and Semimetals* (Elsevier, Amsterdam, 1975), Vol. 10, pp. 1–89.

[38] A. Verma, A. P. Kajdos, T. A. Cain, S. Stemmer, and D. Jena, Phys. Rev. Lett. **112**, 216601 (2014).

[39] E. Yagi, R. R. Hasiguti, and M. Aono, Phys. Rev. B **54**, 7945 (1996).

[40] J.-J. Zhou and M. Bernardi, arXiv:1905.03414.